

Precise measurement of $\Gamma(K_S \rightarrow \pi^+\pi^-(\gamma))/\Gamma(K_S \rightarrow \pi^0\pi^0)$ with the KLOE detector at DAΦNE

F. Ambrosino,¹ A. Antonelli,² M. Antonelli,² C. Bacci,³ P. Beltrame,⁴ G. Bencivenni,² S. Bertolucci,² C. Bini,⁵ C. Bloise,² V. Bocci,⁵ F. Bossi,² D. Bowring,⁶ P. Branchini,³ R. Caloi,⁵ P. Campana,² G. Capon,² T. Capussela,¹ F. Ceradini,³ S. Chi,² G. Chiefari,¹ P. Ciambri,² S. Conetti,⁶ E. De Lucia,² A. De Santis,⁵ P. De Simone,² G. De Zorzi,⁵ S. Dell'Agnello,² A. Denig,⁴ A. Di Domenico,⁵ C. Di Donato,¹ S. Di Falco,⁷ B. Di Micco,³ A. Doria,¹ M. Dreucci,² G. Felici,² A. Ferrari,² M. L. Ferrer,² G. Finocchiaro,² S. Fiore,⁵ C. Forti,² P. Franzini,⁵ C. Gatti,² P. Gauzzi,⁵ S. Giovannella,² E. Gorini,⁸ E. Graziani,³ M. Incagli,⁷ W. Kluge,⁴ V. Kulikov,⁹ F. Lacava,⁵ G. Lanfranchi,² J. Lee-Franzini,^{2,10} D. Leone,⁴ M. Martini,² P. Massarotti,¹ W. Mei,² S. Meola,¹ S. Miscetti,² M. Moulson,² S. Müller,² F. Murtas,² M. Napolitano,¹ F. Nguyen,³ M. Palutan,² E. Pasqualucci,⁵ A. Passeri,³ V. Patera,^{2,11} F. Perfetto,¹ L. Pontecorvo,⁵ M. Primavera,⁸ P. Santangelo,² E. Santovetti,¹² G. Saracino,¹ B. Sciascia,² A. Sciubba,^{2,11} F. Scuri,⁷ I. Sfiligoi,² T. Spadaro,² M. Testa,⁵ L. Tortora,³ P. Valente,² B. Valeriani,⁴ G. Venanzoni,² S. Veneziano,⁵ A. Ventura,⁸ R. Versaci,² and G. Xu^{2,13}

(The KLOE Collaboration)

¹*Dipartimento di Scienze Fisiche dell'Università "Federico II" e Sezione INFN, Napoli, Italy*

²*Laboratori Nazionali di Frascati dell'INFN, Frascati, Italy*

³*Dipartimento di Fisica dell'Università e Sezione INFN, "Roma Tre", Italy*

⁴*Institut für Experimentelle Kernphysik, Universität Karlsruhe, Germany*

⁵*Dipartimento di Fisica dell'Università e Sezione INFN, "La Sapienza", Italy*

⁶*Physics Department, University of Virginia, Charlottesville, VA, USA*

⁷*Dipartimento di Fisica dell'Università e Sezione INFN, Pisa, Italy*

⁸*Dipartimento di Fisica dell'Università e Sezione INFN, Lecce, Italy*

⁹*Permanent address: Institute for Theoretical and Experimental Physics, Moscow, Russia*

¹⁰*Physics Department, State University of New York at Stony Brook, NY, USA*

¹¹*Dipartimento di Energetica dell'Università "La Sapienza", Roma, Italy*

¹²*Dipartimento di Fisica dell'Università e Sezione INFN, "Tor Vergata", Italy*

¹³*Permanent address: Institute of High Energy Physics, CAS, Beijing, China*

Using a sample of over 400 million $\phi \rightarrow K_S K_L$ decays produced during the years 2001 and 2002 at the DAΦNE e^+e^- collider, the ratio $R_S^\pi = \Gamma(K_S \rightarrow \pi^+\pi^-(\gamma))/\Gamma(K_S \rightarrow \pi^0\pi^0)$ has been measured with the KLOE detector. The result is $R_S^\pi = 2.2555 \pm 0.0012_{\text{stat}} \pm 0.0021_{\text{syst-stat}} \pm 0.0050_{\text{syst}}$, which is in good agreement with the previously published result based on the KLOE data sample from the year 2000. The average of the KLOE results is $R_S^\pi = 2.2549 \pm 0.0054$, reducing the total error by a factor of three, to 0.25%.

PACS numbers: 13.25.Es, 14.40.Aq

I. INTRODUCTION

The ratio $R_S^\pi = \Gamma(K_S \rightarrow \pi^+\pi^-(\gamma))/\Gamma(K_S \rightarrow \pi^0\pi^0)$ is a fundamental parameter of the K_S meson. Since the sum of the branching ratios (BR's) for the two dominant decays of the short-lived neutral kaon differs from unity by just 10^{-3} , the measurement of R_S^π provides the BR's for $K_S \rightarrow \pi^0\pi^0$ and $K_S \rightarrow \pi^+\pi^-(\gamma)$ with only small corrections. The latter BR is a convenient normalization for the BR's of all other K_S decays to charged particles. In particular, it is used to obtain $\Gamma(K_S \rightarrow \pi e \nu)$, which is of interest in testing many predictions of the Standard Model, as discussed in Ref. 1. From R_S^π one can also derive phenomenological parameters of the kaon system such as the relative magnitude and phase of the $I=0$ and $I=2$ $\pi\pi$ -scattering amplitudes. Isospin-breaking effects and radiative corrections to the scattering amplitudes are discussed in Refs. 2, 3. Finally, R_S^π enters into the double ratio that quantifies direct CP violation in $K \rightarrow \pi\pi$

transitions:

$$R_S^\pi/R_L^\pi = 1 - 6\Re(\epsilon'/\epsilon), \quad (1)$$

where $R_L^\pi = \Gamma(K_L \rightarrow \pi^+\pi^-(\gamma))/\Gamma(K_L \rightarrow \pi^0\pi^0)$. The most accurate measurement of R_S^π to date was performed by KLOE using data collected in 2000 for an integrated luminosity of $\sim 17 \text{ pb}^{-1}$: $R_S^\pi = 2.236 \pm 0.003_{\text{stat}} \pm 0.015_{\text{syst}}$ [4]. This result, which was more precise than the PDG average at the time [5], for the first time properly included photon radiation and increased the PDG value for $\text{BR}(K_S \rightarrow \pi^+\pi^-(\gamma))$ by 0.5% [6]. The overall accuracy of the previous result, 0.7%, was limited by systematic uncertainties. The present result is based on the analysis of 410 pb^{-1} of integrated luminosity acquired during the years 2001 and 2002, and improves on the total error by a factor of three, to 0.25%.

The paper is organized as follows. In the next section, a brief description of the KLOE detector is given. In Section III, the selection criteria for the decays of interest are summarized. In Section IV, a general description of

the scheme used to evaluate the efficiency corrections is given, followed by a detailed discussion on the tagging efficiencies, acceptances, and trigger efficiencies. The result of the analysis is presented in Section V.

II. EXPERIMENTAL SETUP

The data were collected with the KLOE detector at DAΦNE, the Frascati ϕ factory. DAΦNE is an e^+e^- collider that operates at a center-of-mass energy of ~ 1020 MeV, the mass of the ϕ meson. Positron and electron beams of equal energy collide at an angle of $\pi - 25$ mrad, producing ϕ mesons with a small momentum in the horizontal plane: $p_\phi \sim 13$ MeV/c. ϕ mesons decay $\sim 34\%$ of the time into nearly collinear $K^0\bar{K}^0$ pairs. Because $J^{PC}(\phi) = 1^{--}$, the kaon pair is in an antisymmetric state, so that the final state is always $K_S K_L$. The contamination from $K_L K_L$ and $K_S K_S$ final states is negligible for the purposes of this measurement [7, 8, 9]. Therefore, the detection of a K_L signals the presence of a K_S of known momentum and direction, independently of its decay mode. This technique is called K_S tagging in the following. A total of ~ 1.3 billion ϕ mesons were produced, yielding ~ 430 million $K_S K_L$ pairs.

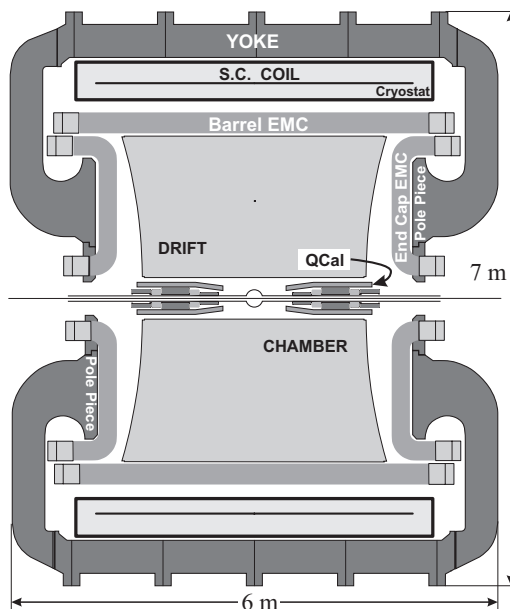


FIG. 1: Vertical cross section of the KLOE detector.

The KLOE detector (Fig.1) consists of a large cylindrical drift chamber (DC) surrounded by a lead/scintillating-fiber sampling calorimeter (EMC). A superconducting coil surrounding the calorimeter provides a 0.52 T magnetic field. The drift chamber [10], which is 4 m in diameter and 3.3 m long, has 12,582 all-stereo tungsten sense wires and 37,746 aluminum field wires. The chamber shell is made of carbon-fiber/epoxy

composite, and the gas used is a 90% helium, 10% isobutane mixture. These features maximize transparency to photons and reduce $K_L \rightarrow K_S$ regeneration and multiple scattering. The DC position resolutions are $\sigma_{xy} \approx 150 \mu\text{m}$ and $\sigma_z \approx 2$ mm. The momentum resolution is $\sigma(p_\perp)/p_\perp \approx 0.4\%$. Vertices are reconstructed with a spatial resolution of ~ 3 mm. The amount of material traversed before particles enter the DC volume affects the detection efficiency for K_S decay products. Particles traverse the beam pipe and the inner DC wall, which are made of a 500 μm -thick layer of Albemet alloy (60% Al-40% Be) and a 800 μm -thick layer of carbon-fiber/epoxy composite aluminized on each side with a foil of 100 μm . The total amount of material corresponds to $\sim 0.5\% X_0$ and to an average conversion probability of $\sim 0.4\%$ for each photon from a $K_S \rightarrow \pi^0\pi^0$ decay. Moreover, assuming a disappearance (including absorption, charge exchange, and inelastic processes) cross section of 400 mb for π^\pm with $p = 200$ MeV/c interacting on carbon [11], and using the same value for beryllium and aluminum, the average probability of disappearance for each pion emitted from a $K_S \rightarrow \pi^+\pi^-(\gamma)$ decay is $\sim 0.5\%$.

The calorimeter [12] is divided into a barrel and two endcaps, contains a total of 88 modules, and covers 98% of the solid angle. The modules are read out at both ends by photomultiplier tubes. The arrival times of particles and the three-dimensional positions of the energy deposits are determined from the signals at the two ends. The readout granularity is $\sim 4.4 \times 4.4 \text{ cm}^2$; the 2440 “cells” are arranged in five layers. Cells close in time and space are grouped into a “calorimeter cluster.” For each cluster, the energy E_{cl} is the sum of the cell energies, and the time t_{cl} and position \mathbf{r}_{cl} are calculated as energy-weighted averages over the fired cells. The energy and time resolutions are $\sigma_E/E = 5.7\%/\sqrt{E(\text{GeV})}$ and $\sigma_t = 57 \text{ ps}/\sqrt{E(\text{GeV})} \oplus 100 \text{ ps}$, respectively.

Only the calorimeter trigger [13] is used for the present measurement. This requires two local energy deposits (trigger sectors) above a threshold of 50 MeV in the barrel and 150 MeV in the endcaps. Events with only two fired trigger sectors in the same endcap are rejected, because this topology is dominated by machine background. A single particle hitting the calorimeter barrel and releasing enough energy to fire two contiguous sectors generates a valid trigger.

Recognition and rejection of cosmic-ray events is also performed at the trigger level: events with two energy deposits above a 30 MeV threshold in the outermost calorimeter plane are rejected as cosmic-ray events. Moreover, to reject residual cosmic rays and machine background events an offline software filter (FILFO) exploits calorimeter and DC information before tracks are reconstructed [14].

The trigger has a large time spread with respect to the beam crossing time. However, it is synchronized with the machine RF divided by 4, $T_{\text{sync}} \sim 10.8$ ns, with an accuracy of 50 ps. The time of the bunch crossing producing an event is determined offline during event reconstruction.

tion.

The response of the detector to the decays of interest and the various backgrounds were studied by using the KLOE Monte Carlo (MC) simulation program [14]. Changes in the machine operation and background conditions are simulated on a run-by-run basis to improve agreement with data when averaged over the sample. The most important parameters are the beam energies and the crossing angle, which are obtained from the analysis of Bhabha scattering events with e^\pm polar angles above 45 degrees. The average value of the center-of-mass energy is evaluated with a precision of 30 keV for each 100 nb^{-1} of integrated luminosity.

Particularly important for correct evaluation of the acceptance for $\pi^+\pi^-$ and $\pi^0\pi^0$ events is the rate of accidental clusters from the machine (R_{acc}). This is extracted from the analysis of $e^+e^- \rightarrow \gamma\gamma$ events, where the low-energy and out-of-time hits due to machine background are easily separated from the two 510 MeV photon clusters.

For the present analysis, an MC sample of $\phi \rightarrow K_S K_L$ decays that corresponds to an integrated luminosity of $\sim 550 \text{ pb}^{-1}$ is used; for the other ϕ -meson final states, an MC sample equivalent to $\sim 90 \text{ pb}^{-1}$ of integrated luminosity has been used.

III. SIGNAL SELECTION

The mean decay lengths of the K_S and K_L are $\lambda_S \sim 0.6 \text{ cm}$ and $\lambda_L \sim 350 \text{ cm}$, respectively. About 50% of K_L 's therefore reach the calorimeter before decaying. The K_L interaction in the calorimeter barrel (K_L crash, K_{cr} in the following) is identified by requiring a cluster of energy above a given threshold E_{cr} not associated with any track, and whose time corresponds to a velocity $\beta = r_{\text{cl}}/ct_{\text{cl}}$ compatible with the kaon velocity in the ϕ center of mass, $\beta^* \sim 0.216$, after the residual ϕ motion is considered. Events with clusters with $0.17 \leq \beta^* \leq 0.28$ are selected. These K_{cr} events are used to tag a K_S “beam” of known momentum. The K_S trajectory is determined with an angular resolution of 1° and the K_S momentum is evaluated with a resolution better than $2 \text{ MeV}/c$ from $\mathbf{p}_{K_S} = \mathbf{p}_\phi - \mathbf{p}_{K_L}$, where the K_L momentum \mathbf{p}_{K_L} is calculated by using the values of the center-of-mass energy and of the ϕ momentum \mathbf{p}_ϕ , and the position of the K_{cr} cluster.

The interaction time, which must be known for the measurement of the cluster times, is obtained from the first particle reaching the calorimeter (pions or photons for the events of interest) assuming a velocity $\beta=1$. This definition of interaction time (T_0 in the following) does not require the K_S decay to be identified when applying the tagging algorithm. In order to reduce the probability that T_0 is accidentally determined from a particle due to machine background, the T_0 is required to be given by a cluster with energy $E_{\text{cl}} > 50 \text{ MeV}$ and distance to the beam line $\rho_{\text{cl}} > 60 \text{ cm}$. This is referred to as a “ T_0

cluster.”

$K_S \rightarrow \pi^+\pi^-(\gamma)$ events are selected by requiring the presence of two tracks of opposite charge with their point of closest approach to the origin inside a cylinder 4 cm in radius and 10 cm in length along the beam line. The tracks momenta and polar angles must satisfy the fiducial cuts $120 \leq p \leq 300 \text{ MeV}/c$ and $30^\circ \leq \theta \leq 150^\circ$. The tracks must also reach the EMC without spiralling, and at least one of them must have an associated T_0 cluster.

$K_S \rightarrow \pi^0\pi^0$ events are identified by the prompt photon clusters from π^0 decays. A prompt photon cluster must satisfy $|t_{\text{cl}} - r_{\text{cl}}/c| \leq 5\sigma_t$, σ_t being the energy-dependent time resolution, and must not be associated to any track. Machine background is reduced by cuts on the cluster energy and polar angle: $E_{\text{cl}} > 20 \text{ MeV}$ and $|\cos\theta| < 0.9$. To accept a $K_S \rightarrow \pi^0\pi^0$ event, three or more prompt photons are required.

The numbers N of $\pi^+\pi^-$ and $\pi^0\pi^0$ events and the corresponding selection efficiencies ϵ_{sel} are then used to compute R_S^π :

$$R_S^\pi = \frac{N(\pi^+\pi^-)}{N(\pi^0\pi^0)} \frac{\epsilon_{\text{sel}}(\pi^0\pi^0)}{\epsilon_{\text{sel}}(\pi^+\pi^-)} \frac{C(\pi^+\pi^-)}{C(\pi^0\pi^0)}, \quad (2)$$

where C is the purity of the sample (the fraction of selected events that are signal), as evaluated from MC.

IV. EFFICIENCY EVALUATION

A. General scheme

The fractional statistical error from the counting is $\sim 0.5 \times 10^{-3}$; the overall uncertainty is dominated by systematics. Therefore, in the analysis, great effort has been put into carefully estimating all possible systematic effects, as discussed in detail in Ref. 15.

The selection efficiency is expressed for each of the two channels ($\pi^+\pi^-$, $\pi^0\pi^0$) as follows:

$$\epsilon_{\text{sel}} = \epsilon_{\text{tag+acc}} \epsilon_{\text{trg}} \epsilon_{\text{CV}} \epsilon_{\text{FILFO}}, \quad (3)$$

where $\epsilon_{\text{tag+acc}}$ is the joint efficiency for reconstructing both the tagging K_L interaction and the K_S decay; ϵ_{trg} , ϵ_{CV} , and ϵ_{FILFO} are the efficiencies for the trigger, the cosmic-ray veto, and the offline background filter (FILFO). The tagging efficiency and the signal acceptance are correlated by the T_0 determination, and cannot be simply factorized, as discussed below.

For essentially all of selected $K_S \rightarrow \pi^0\pi^0$ events, the T_0 corresponds to the true collision time: if this is not the case, the prompt photon cluster selection fails and the event is lost. For the purposes of K_{cr} selection, the velocity β^* is therefore correctly evaluated (open histogram of Fig. 2). In contrast, for most $K_S \rightarrow \pi^+\pi^-$ events, the T_0 does not correspond to the true collision time. Most charged pions arrive at the EMC $\sim 3 \text{ ns}$ later than γ 's from π^0 decays and the time T_0 is therefore delayed by one RF period, $T_{\text{RF}} \sim 2.7 \text{ ns}$; in a few percent of the

cases, larger displacements are observed. This results in a $\sim 10\%$ overestimation of the K_L velocity and a difference in the tail populations (shaded histogram of Fig. 2). The displacement of the two β^* distributions within the accepted β^* region affects the tagging efficiency, which then differs for each of the two final states. In order to parametrize this effect, two classes of events are defined: events selected by the K_{cr} algorithm on the basis of the true value of the collision time are called $K_{\text{cr}}^{\text{true}}$, the rejected ones are non- $K_{\text{cr}}^{\text{true}}$. While all of $K_S \rightarrow \pi^0\pi^0$ events are $K_{\text{cr}}^{\text{true}}$, the net effect due to incorrect T_0 determination on the tagging efficiency for $K_S \rightarrow \pi^+\pi^-$ events is that a fraction $(1 - A) \sim 3\%$ of $K_{\text{cr}}^{\text{true}}$ is lost, while a fraction $B \sim 0.3\%$ of non- $K_{\text{cr}}^{\text{true}}$ creeps into the selection (the fractions A and B are defined more precisely in Sec. IV B).

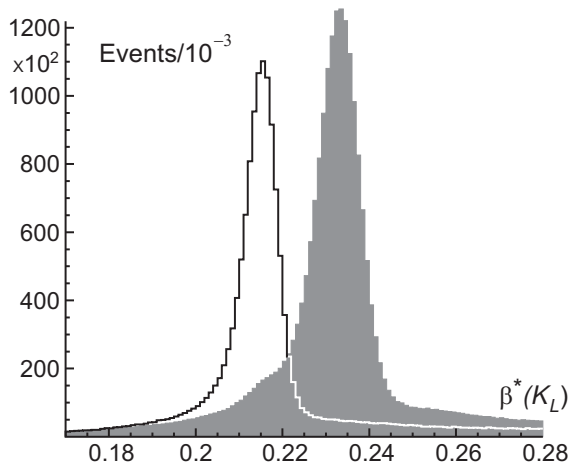


FIG. 2: K_L velocity transformed to the ϕ rest frame, β^* , for $K_S \rightarrow \pi^0\pi^0$ (open histogram) and $K_S \rightarrow \pi^+\pi^-$ (shaded histogram). The range shown corresponds to the accepted window in β^* .

Furthermore, $K_{\text{cr}}^{\text{true}}$ and non- $K_{\text{cr}}^{\text{true}}$ events have different topologies: the first category is dominated by real K_L interactions in the EMC, with β^* lying around the peak; the second category is mostly due to in-flight K_L decays before the EMC. These two topologies also correspond to different K_L energy releases in the EMC, the latter topology being much softer than the former (Fig. 3). If the K_{cr} tag is selected using a low value for the minimum energy cut ($E_{\text{cr}} = 125$ MeV), there is substantial contamination from in-flight K_L decays occurring before the EMC. This is shown by the MC distribution of the transverse position (ρ_L) corresponding to the K_L decay or interaction producing the K_{cr} cluster (Fig. 4). This contamination completely disappears when the cut is increased to 300 MeV. Due to interference between K_L and K_S decay products, which undermines K_S reconstruction performance, the K_S signal acceptance is a function of the K_L decay mode and of the position ρ_L (Fig. 5). Therefore, the signal acceptance a_{cr} for the $K_{\text{cr}}^{\text{true}}$ events, which are dominated by K_L interactions in the EMC, is

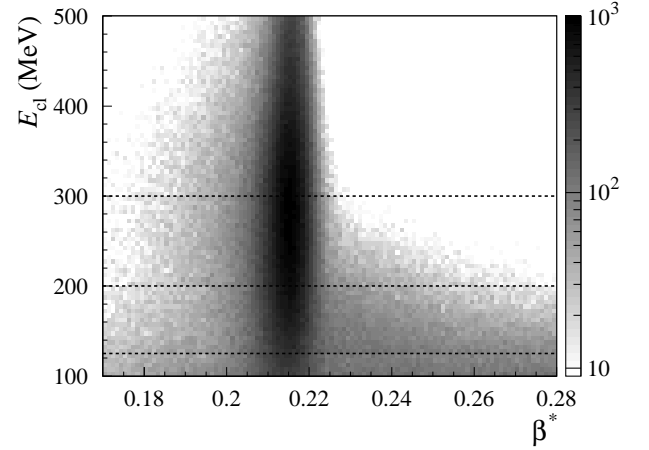


FIG. 3: K_{cr} cluster energy versus β^* for $K_S \rightarrow \pi^0\pi^0$ events. The dashed lines correspond to the three different cuts on K_{cr} energy used in the analysis.

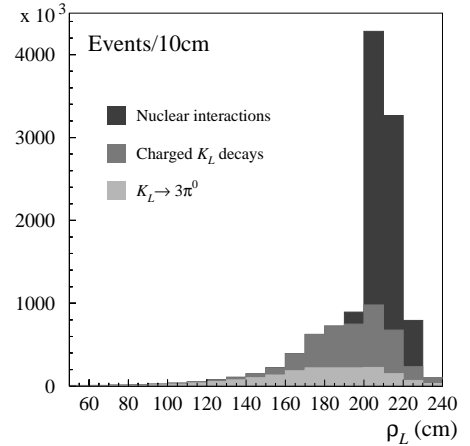


FIG. 4: MC distribution of K_L decay/interaction position ρ_L for $K_{\text{cr}}^{\text{true}}$ events selected with $E_{\text{cr}} = 125$ MeV; contributions from $K_L \rightarrow \pi^0\pi^0\pi^0$, from K_L decays to charged particles, and from nuclear interactions are shown separately.

a few percent higher than that for non- $K_{\text{cr}}^{\text{true}}$ events, $a_{\overline{\text{cr}}}$.

Finally, the selection efficiency of Eq. 3 is expressed by combining the acceptances with the probabilities ϵ_{cr} and $1 - \epsilon_{\text{cr}}$ for having a $K_{\text{cr}}^{\text{true}}$ or non- $K_{\text{cr}}^{\text{true}}$ event, respectively:

$$\epsilon_{\text{sel}} = [\epsilon_{\text{cr}} a_{\text{cr}} A + (1 - \epsilon_{\text{cr}}) a_{\overline{\text{cr}}} B] \epsilon_{\text{trg}} \epsilon_{\text{CV}} \epsilon_{\text{FILFO}}. \quad (4)$$

The fractions A and B are evaluated using data control samples, while the efficiency ϵ_{cr} is taken from MC (Sec. IV B). The acceptances a_{cr} and $a_{\overline{\text{cr}}}$ are evaluated using the MC, with data-driven corrections as explained in Secs. IV C and IV D for $\pi^+\pi^-$ and $\pi^0\pi^0$ events, respectively. The efficiencies ϵ_{trg} , ϵ_{CV} , and ϵ_{FILFO} are evaluated using data control samples as discussed in Sec. IV E. All

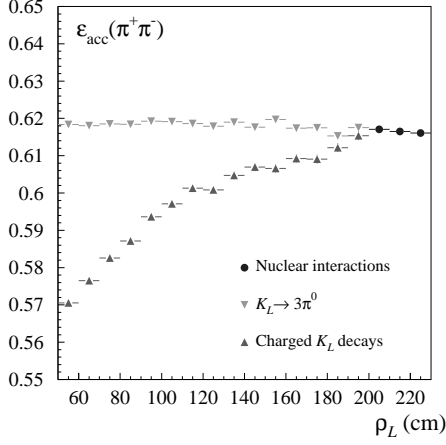


FIG. 5: Acceptance of $K_S \rightarrow \pi^+\pi^-(\gamma)$ as a function of ρ_L , for different K_L decay/interaction channels.

of the efficiencies in Eq. 4 are to be understood as conditional probabilities, with each defined relative to the sample from the previous step in the analysis, according to the order in which they are applied.

The analysis is carried out for three different cuts on the K_L cluster energy: $E_{cr} = 125, 200$, and 300 MeV. The tagging efficiencies are very different in each case: $\epsilon_{cr} \sim 0.31, 0.22$, and 0.11 , respectively. The fraction of K_L in-flight decays entering the selection varies significantly as well. Moreover, some of the corrections applied and the related systematic uncertainties vary considerably with the cut value. This allows the robustness of the result to be tested.

The data were divided into 17 different samples following small changes in the machine energy. The large number of events allowed a statistical error at the few per-mil level to be obtained for each single data period. Comparison of the independent measurements from each data sample provides a stringent test of the validity of the corrections for possible variations in the selection efficiency during data taking. Results will be presented for each K_{cr} energy cut, averaging over all 17 samples. The final result is obtained by choosing the value of E_{cr} which minimizes the total error. Numerical details concerning all of the quantities involved in Eqs. 2 and 4 are given in the following sections for a representative sample (no. 10).

B. Tagging efficiencies

This section concerns the evaluation of the quantities involved in the determination of the tagging efficiency: A , B , and ϵ_{cr} .

The following parametrizations are used: $A = \sum_n f_n P_n^{\text{in}}$, $B = \sum_n f_n P_n^{\text{out}}$, where

- f_n is the T_0 spectrum, *i.e.*, the fraction of events in

which T_0 is shifted by $n \times T_{\text{RF}}$ with respect to the true collision time T_0^{true} ;

- P_n^{in} is the probability that, given a found K_{cr}^{true} event, the K_{cr} tag is again found even after the T_0 determination is shifted by $n \times T_{\text{RF}}$;
- P_n^{out} is the probability that, in the absence of a found K_{cr}^{true} event, a K_{cr} tag is newly found after the T_0 determination is shifted by $n \times T_{\text{RF}}$.

All of these quantities are taken from data control samples.

The T_0 spectrum (f_n) is evaluated for both $\pi^+\pi^-$ and $\pi^0\pi^0$ events after the signal selection requests have been applied. For the charged mode, a subsample of $K_S \rightarrow \pi^+\pi^-$ events is selected in which both charged pions are associated to clusters. For each pion, an estimate of T_0^{true} is obtained from the cluster time and the time of flight calculated from the track parameters. The robustness of this estimate is increased by requiring that both pions give the same result. The f_n spectrum is obtained as the normalized distribution of $(T_0 - T_0^{\text{true}})/T_{\text{RF}}$ (Fig. 6). As previously mentioned, T_0 overestimates the true collision time by one RF period $\sim 97\%$ of the time. The negative tail of the spectrum shows peaks corresponding to the bunch-crossing times, and is dominated by events in which T_0 is determined by a cluster from machine background occurring at random with respect to the collision time. For $\pi^0\pi^0$ events the situation is

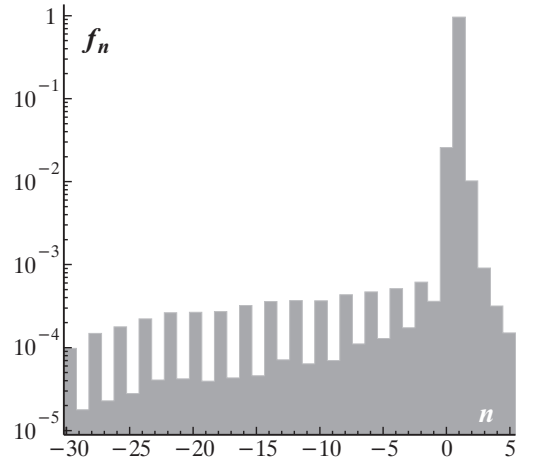


FIG. 6: f_n spectrum for $K_S \rightarrow \pi^+\pi^-$ events.

much simpler, because the request of having at least three prompt clusters is fulfilled only if $T_0 = T_0^{\text{true}}$. Therefore f_n is negligible for $n \neq 0$, and the values $A(\pi^0\pi^0) = 1$ and $B(\pi^0\pi^0) = 0$ are used.

For the charged mode, the probabilities P_n^{in} and P_n^{out} are needed for the evaluation of A and B . For this purpose, a sample of events selected on the basis of a reconstructed $K_S \rightarrow \pi^+\pi^-$ decay (without reference to the K_{cr} tag) is used. The estimate of the true collision time T_0^{true} described above is used to divide these events into K_{cr}^{true}

and non- $K_{\text{cr}}^{\text{true}}$. The T_0 value is then artificially shifted by $n \times T_{\text{RF}}$ with respect to T_0^{true} . For $K_{\text{cr}}^{\text{true}}$ events, the probability P_n^{in} of still finding the K_{cr} is evaluated, as is the probability P_n^{out} of finding a K_{cr} not originally present for non- $K_{\text{cr}}^{\text{true}}$ events. The probabilities P_n^{in} and P_n^{out} are shown as a function of the T_0 shift in Fig. 7. From the probabilities f_n , P_n^{in} , and P_n^{out} the fractions

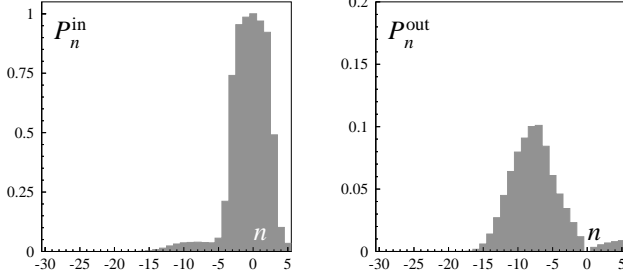


FIG. 7: Probabilities P_n^{in} (left) and P_n^{out} (right) as a function of the T_0 shift (n). By definition, $P_0^{\text{in}}=1$ and $P_0^{\text{out}}=0$.

A and B are calculated. The results for $\pi^+\pi^-$ events are listed in Tab. I. The value of $A(\pi^+\pi^-)$ increases with E_{cr} , reaching $\sim 99\%$ for $E_{\text{cr}}=300$ MeV. The tails of the β^* spectrum are indeed suppressed by increasing the K_{cr} energy cut, as shown in Fig. 3. This reduces the acceptance losses due to incorrect T_0 determination. The maximal variation of $A(\pi^+\pi^-)$ during data taking is $\sim 1\%$.

Possible biases in the estimate of the f_n spectra have been checked using the MC, by evaluating the ratio A^{true}/A . Here, A^{true} is evaluated from MC truth and A is evaluated with the same method used for data. The above ratio is applied as a correction to the estimate of A for data; the systematic error, taken as 100% of the correction, amounts to 0.25×10^{-3} for $E_{\text{cr}}=300$ MeV. Given the small value of $B(\pi^+\pi^-)$, no correction is applied. A similar comparison with MC truth allows a systematic error of $\sim 0.4 \times 10^{-3}$ to be assigned to the assumption $A(\pi^0\pi^0)=1$. The total systematic error from the evaluation of the f_n spectra and of the probabilities P_n^{in} , P_n^{out} is 0.45×10^{-3} at $E_{\text{cr}}=300$ MeV (see Tab. V).

When computing the ratio between $\pi^+\pi^-$ and $\pi^0\pi^0$ selection efficiencies (see Eqs. 2 and 4) the values of the $K_{\text{cr}}^{\text{true}}$ efficiencies $\epsilon_{\text{cr}}(\pi^+\pi^-)$ and $\epsilon_{\text{cr}}(\pi^0\pi^0)$ are needed; since $B(\pi^+\pi^-) \sim 0.3\%$ and $B(\pi^0\pi^0)=0$, the ratio of selection efficiencies depends on the ratio $\epsilon_{\text{cr}}(\pi^+\pi^-)/\epsilon_{\text{cr}}(\pi^0\pi^0)$ rather than on the ϵ_{cr} values for each channel. This ratio varies with E_{cr} , ranging from ~ 1.003 at 125 MeV up to ~ 1.014 at 300 MeV (Tab. I). This is due to the geometrical overlap in the EMC between K_S daughter particles and the K_L , which affects the K_{cr} reconstruction efficiency in a manner dependent on the decay channel. For $\pi^+\pi^-$ events, the $K_{\text{cr}}^{\text{true}}$ efficiency drops when the pions get closer to the K_L because of the higher probability of associating the K_L cluster to one pion track; for $\pi^0\pi^0$ events, a drop is observed when a K_S photon and the K_L hit the same calorimeter cell, thus

spoiling the cluster reconstruction. These effects have been studied using MC control samples of signal events in which at least one K_S decay product reaches the EMC barrel. The effects are then visible in the dependence of $\epsilon_{\text{cr}}(\pi^+\pi^-)$ on the minimum distance d_{min} between the K_L and the closest K_S decay product on the barrel and in the dependence of $\epsilon_{\text{cr}}(\pi^0\pi^0)$ on the minimum angular distance $\Delta\phi_{\text{min}}$ in the transverse plane (Fig. 8). Biases are present only when K_S daughter particles enter the EMC close to the K_L impact point. The reliability of

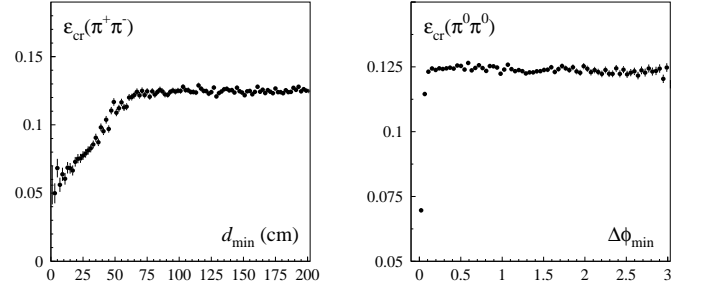


FIG. 8: $\epsilon_{\text{cr}}(\pi^+\pi^-)$ as a function of d_{min} (left) and $\epsilon_{\text{cr}}(\pi^0\pi^0)$ as a function of $\Delta\phi_{\text{min}}$ (right), for $E_{\text{cr}}=300$ MeV. The efficiencies shown have been obtained using control samples of signal events in which at least one K_S decay product reaches the barrel.

the MC in reproducing this overlap effect is checked by comparing data and MC distributions of d_{min} and $\Delta\phi_{\text{min}}$ for events with a K_{cr} tag found (Fig. 9). The ratio of data and MC distributions is constant in the region safe from overlap effects. A significant discrepancy is only present for $\pi^+\pi^-$ events when $d_{\text{min}} < 10$ cm. The MC evaluation of $\epsilon_{\text{cr}}(\pi^+\pi^-)/\epsilon_{\text{cr}}(\pi^0\pi^0)$ is corrected by scaling the number of K_{cr} events found for small d_{min} values according to the ratio measured for data. The systematic error, taken as 100% of the correction, amounts to $\sim 0.44 \times 10^{-3}$ for $E_{\text{cr}}=300$ MeV (Tab. V).

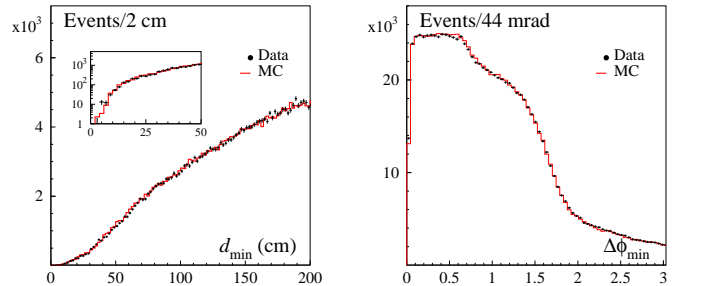


FIG. 9: Comparison between data and MC distributions of d_{min} for $\pi^+\pi^-$ events (left) and $\Delta\phi_{\text{min}}$ for $\pi^0\pi^0$ events (right).

E_{cr} value		125 MeV	200 MeV	300 MeV
$\pi^+\pi^-$	A	0.9634(1)	0.9866(1)	0.9933(1)
	$B(\times 10^{-3})$	3.4489(6)	1.6675(1)	0.71563(3)
	ϵ_{cr}	0.3106(2)	0.2231(2)	0.1082(2)
$\pi^0\pi^0$	ϵ_{cr}	0.3097(3)	0.2217(3)	0.1067(2)

TABLE I: Tagging probabilities entering into the evaluation of the selection efficiency (Eq. 4) for $\pi^+\pi^-$ and $\pi^0\pi^0$ events, for data sample no. 10 and minimum K_{cr} energies of 125, 200, and 300 MeV. Statistical errors on the last digit are shown in parentheses.

C. Acceptance and purity for $K_S \rightarrow \pi^+\pi^-(\gamma)$

The $\pi^+\pi^-$ acceptance is evaluated from MC. Since no cut is applied on the $\pi\pi$ invariant mass, the selection includes $K_S \rightarrow \pi^+\pi^-\gamma$ events with photon energies up to the end point (~ 160 MeV in the K_S rest frame). However, due to the fact that both pion tracks must extrapolate to the calorimeter without spiralling, the acceptance depends on the photon energy: the harder the photon in the final state, the higher the probability that one of the pion tracks spirals in the chamber before reaching the EMC. The MC simulation includes final-state radiation [16]. The acceptance obtained by MC is shown in Fig. 10 as a function of the photon energy E_γ^* in the K_S rest frame. The simulated spectrum is

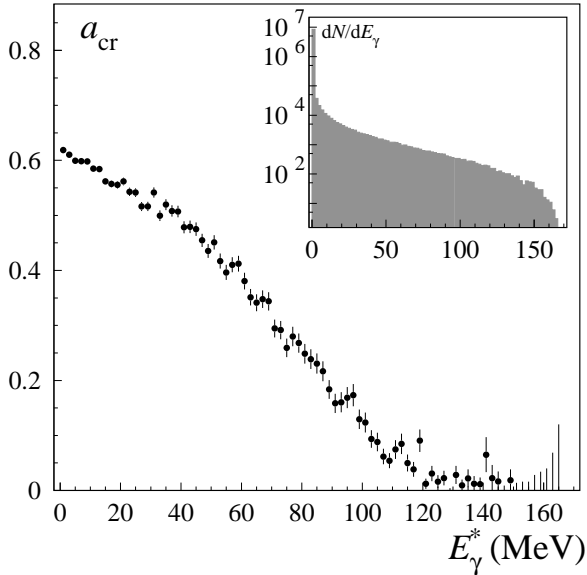


FIG. 10: Acceptance a_{cr} for $K_S \rightarrow \pi^+\pi^-(\gamma)$ as a function of the center-of-mass photon energy. The photon spectrum used in the simulation is shown in the inset.

also shown in the inset of Fig. 10. The fraction of events with $E_\gamma^* > 20$ and 50 MeV are 7.0×10^{-3} and 2.5×10^{-3} , respectively, in excellent agreement with the measured

values $(7.10 \pm 0.22) \times 10^{-3}$ and $(2.56 \pm 0.09) \times 10^{-3}$ [17]. The MC calculation thus provides a fully inclusive acceptance, which is $\sim 0.3\%$ lower than that obtained with a pure $K_S \rightarrow \pi^+\pi^-$ simulation.

A crucial issue when evaluating the $\pi^+\pi^-$ acceptance is to correctly reproduce the DC tracking efficiency, including all possible variations correlated with the level of machine background and with the hardware performance of the apparatus. For this purpose, accidental background hits in the DC are extracted from real $e^+e^- \rightarrow \gamma\gamma$ events and are overlaid with the simulated events; moreover, the measured hardware hit efficiency is used to sample the MC hit generation [14]. To take into account residual differences in the tracking efficiencies for data and MC, the acceptance calculation is performed by weighting the contribution of each single pion with the ratio $\epsilon_{\text{trk}}^{\text{data}}/\epsilon_{\text{trk}}^{\text{MC}}$. The single-track efficiencies ϵ_{trk} for data and MC are evaluated from a subsample of $K_S \rightarrow \pi^+\pi^-$ events tagged by a K_{cr} . Using the K_S momentum \mathbf{p}_{K_S} as determined from \mathbf{p}_ϕ and by the K_L flight direction, it is indeed possible to identify the $\pi^+\pi^-$ final state by selecting a single pion track (“tagging” track) with the expected momentum in the K_S rest frame: $201 \leq p_{\text{tag}}^* \leq 209$ MeV/c. This selection reduces background to a negligible level, while at the same time providing a good estimate of the momentum of the other pion: $\mathbf{p}_{\text{other}} = \mathbf{p}_{K_S} - \mathbf{p}_{\text{tag}}$. The single-track efficiency is then obtained by counting the fraction of times in which a second pion track is found; it is evaluated in bins of transverse and longitudinal momenta, separately for each particle charge. This method takes into account not only differences in ϵ_{trk} for data and MC, but also differences between the real and simulated nuclear interaction cross sections for the pions.

The MC calculation is also corrected for data-MC differences in the efficiency ϵ_{T_0} for a single pion with impact on the calorimeter to provide a T_0 cluster. This is evaluated using various data control samples ($K_S \rightarrow \pi^+\pi^-$, $\phi \rightarrow \pi^+\pi^-\pi^0$) as a function of the track momentum and the angle of incidence on the EMC, distinguishing between π^+ and π^- tracks (or μ^+ and μ^- tracks, in case of in-flight pion decays), and separately treating tracks reaching the barrel or the endcaps.

The values of a_{cr} and $a_{\overline{\text{cr}}}$ are listed in Tab. II, together with the number of events selected as $\pi^+\pi^-$. The errors quoted on a_{cr} and $a_{\overline{\text{cr}}}$ are due to the statistics of the MC sample and of the control samples used for the efficiency determination. The maximal variation of the acceptance during data taking is $\sim 2\%$, and is due to variations in the machine operating conditions (background levels and center of mass energy). The acceptance $a_{\overline{\text{cr}}}$ is $\sim 3\%$ lower than a_{cr} for all values of E_{cr} , because of the presence of K_L 's decaying into charged particles before reaching the EMC, which disturb the reconstruction of K_S pion tracks as discussed in section IV A. The value of a_{cr} increases by 0.8×10^{-3} as the E_{cr} cut is moved from 125 to 300 MeV. This is due to the contamination from late K_L decays in the $K_{\text{cr}}^{\text{true}}$ sample (Fig. 4), which is suppressed when the K_{cr} energy cut is raised. The above variation is taken

as a conservative estimate of the systematic error from the simulation of this K_S - K_L interference. A further contribution to the systematic error comes from the T_0 efficiency correction, ϵ_{T0} ; it is estimated by MC as the difference between the result of the method described above and the MC truth. A non-zero difference is found and is ascribed to interference between the two decay products of the K_S , which is not correctly taken into account by the above method. The difference is 1.4×10^{-3} at $E_{cr}=300$ MeV (Tab. V). This value is both applied as a correction and taken as a conservative estimate of the systematic error.

The purity C of the $\pi^+\pi^-$ sample is estimated by MC to be ~ 0.9989 and is independent of E_{cr} (see Tab. II). Two sources contribute to the background contamination: K_S decays to semileptonic final states ($\sim 0.7 \times 10^{-3}$) and $\phi \rightarrow \pi^+\pi^-\pi^0$ decays ($\sim 0.4 \times 10^{-3}$). Semileptonic decays are able to satisfy with high efficiency the loose kinematic criteria used to select $\pi^+\pi^-$ events. Events with $\phi \rightarrow \pi^+\pi^-\pi^0$ decays enter the selection when an early accidental cluster establishes T_0 and one of the two high-energy photons from the π^0 is erroneously selected as the K_{cr} . The systematic error on the purity comes from the uncertainty on the BR's for the decays involved and, for the $\phi \rightarrow \pi^+\pi^-\pi^0$ contribution, from the uncertainty on the rate R_{acc} . The error from these sources is 0.1×10^{-3} at $E_{cr}=300$ MeV (Tab. V).

E_{cr} value	125 MeV	200 MeV	300 MeV
N	1,218,000	907,400	490,900
a_{cr}	0.6187(5)	0.6192(6)	0.6195(8)
$a_{\overline{cr}}$	0.5968(5)	0.5991(5)	0.6016(5)
C	0.99882(4)	0.99891(4)	0.99886(6)

TABLE II: Values for the observed yield, the acceptance, and the purity of the $\pi^+\pi^-$ selection, for data sample no. 10 and minimum K_{cr} energies of 125, 200, and 300 MeV. Statistical errors on the last digit are shown in parentheses.

D. Acceptance and purity for $K_S \rightarrow \pi^0\pi^0$

The $K_S \rightarrow \pi^0\pi^0$ acceptance is evaluated from MC. To take into account data-MC differences in the cluster efficiency ϵ_{cl} for low-energy photons, the acceptance calculation is performed by weighting each photon with the ratio $\epsilon_{cl}(\text{data})/\epsilon_{cl}(\text{MC})$. The single-photon detection efficiencies are evaluated from control samples of $\phi \rightarrow \pi^+\pi^-\pi^0$ events, which are selected using DC information only: two tracks with opposite charge from the interaction point (IP) are required, with a missing four-momentum $p_{\pi^0} = p_\phi - p_{\pi^+} - p_{\pi^-}$ compatible with the π^0 mass hypothesis. A photon from π^0 decay is identified (“tagging” photon, γ_1) as a cluster with time of flight and energy in an appropriate interval around the expected values. The energy is derived from the π^0 momentum

and the position of the cluster for γ_1 using the relation $E_{\gamma_1} = m_{\pi^0}^2/2(E_{\pi^0} - p_{\pi^0} \cos \theta_{\pi^0\gamma_1})$. The above selection provides a good estimate of the momentum of the second photon, $\mathbf{p}_{\gamma_2} = \mathbf{p}_{\pi^0} - \mathbf{p}_{\gamma_1}$. The photon efficiency ϵ_{cl} is then obtained by counting the fraction of times in which the second photon is found in a cone around the expected direction. The result is evaluated in bins in the expected polar angle and energy; photons from $\phi \rightarrow \pi^+\pi^-\pi^0$ events have a wider energy spectrum than that for $K_S \rightarrow \pi^0\pi^0$ events, so that the efficiency can be successfully evaluated up to the end point, $E_\gamma \sim 300$ MeV.

The values of a_{cr} are listed in Tab. III, together with the number of events selected as $\pi^0\pi^0$. The maximal variation in the acceptance during data taking is $\sim 1\%$ and is due to variations in the machine background. The various sources of systematic uncertainty on the acceptance evaluation are discussed below.

A first contribution to the systematic uncertainty on the photon counting arises from uncertainty in the data-MC cluster-efficiency correction. This has been evaluated by varying the cut on the minimum cluster energy, E_{min} , from the default value of 20 MeV to values between 7 and 50 MeV and checking the stability of the number of selected events after efficiency corrections, $n(E_{min})$. When the cut is moved from 7 to 50 MeV, the acceptance decreases by $\sim 18\%$. The data-MC cluster efficiency correction is ~ 0.9965 with the cut at 7 MeV, and is negligible with the cut at 50 MeV. The variation of $n(E_{min})$ normalized to $n(20 \text{ MeV})$ is shown as a function of E_{min} in Fig. 11. The associated fractional systematic error is

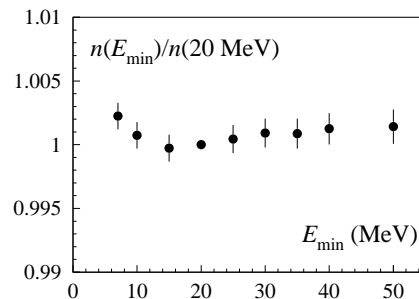


FIG. 11: Variation of the number of $K_S \rightarrow \pi^0\pi^0$ events relative to that for a 20-MeV cut, as a function of the minimum energy cut E_{min} . Each number is obtained correcting the event count with the corresponding efficiency.

0.5×10^{-3} .

An additional systematic uncertainty in photon counting arises from a data-MC difference in the probability for a photon to produce more than one prompt cluster (“splitting”). If this occurs, an event with only two real prompt photons might be accepted as a three-prompt-photon event. The relative bias induced in the acceptance is proportional to the difference between data and

MC splitting probabilities:

$$\frac{\Delta a_{\text{cr}}}{a_{\text{cr}}} = (P_{\text{split}}^{\text{data}} - P_{\text{split}}^{\text{MC}}) \times \frac{2N_2}{N_{\geq 3}}, \quad (5)$$

where N_i ($N_{\geq i}$) represents the number of $K_S \rightarrow \pi^0\pi^0$ events with i ($\geq i$) prompt photons. The splitting probabilities are evaluated for data and MC using events with a K_{cr} and five prompt clusters. In this sample, there is always either one split or one accidental cluster. The splitting probability is then evaluated as $P_{\text{split}} = N_{\text{split}}/(4N_4)$, where N_{split} is the number of five-prompt events in which a pair of clusters closer than 80 cm is found. The results for data and MC are $P_{\text{split}}^{\text{data}} \sim 2.7 \times 10^{-3}$ and $P_{\text{split}}^{\text{MC}} \sim 1.4 \times 10^{-3}$. Given a ratio $N_2/N_{\geq 3} \sim 0.09$, the bias on the acceptance from Eq. 5 is 0.22×10^{-3} ; this is taken both as a correction and as an estimate of the systematic uncertainty due to this effect.

Photons from $K_S \rightarrow \pi^0\pi^0$ have a probability of $\sim 4 \times 10^{-3}$ to convert to an e^+e^- pair before entering the DC volume. Moreover, there is a probability of $\sim 2.4\%$ that at least one π^0 undergoes a Dalitz decay [6]. These two categories of events produce at most three prompt clusters and are therefore selected with a lower efficiency $a_{\text{cr}}^{\text{pair}} \sim 0.67$ instead of $a_{\text{cr}} \sim 0.89$. The $\pi^0\pi^0$ acceptance, which is averaged over the populations with and without e^+e^- pairs in the final state is therefore subject to error if the MC does not reproduce the real γ -conversion cross section (the uncertainty due to the BR for the Dalitz decay is negligible). This effect has been checked by searching for tracks from the IP in events selected as $\pi^0\pi^0$ in data and MC. If an e^+e^- pair is produced, at least one track is reconstructed with a probability $p_{\text{trk}} \sim 0.74$. Having measured for data and MC the fraction f_{trk} of events with at least one track pair from the IP, the correction to the acceptance is evaluated as follows:

$$\frac{\Delta a_{\text{cr}}}{a_{\text{cr}}} = \frac{f_{\text{trk}}^{\text{data}} - f_{\text{trk}}^{\text{MC}}}{p_{\text{trk}} a_{\text{cr}}^{\text{pair}}} \times (a_{\text{cr}} - a_{\text{cr}}^{\text{pair}}). \quad (6)$$

The difference $f_{\text{trk}}^{\text{data}} - f_{\text{trk}}^{\text{MC}}$ is $\sim 10^{-3}$. This results in a 0.38×10^{-3} bias on the acceptance, which is taken both as a correction and as an estimate of the systematic uncertainty due to photon conversion.

The total systematic error on the acceptance due to “cluster counting” effects is therefore 0.66×10^{-3} at $E_{\text{cr}} = 300$ MeV (Tab. V).

In addition to the above effects, the consequences of possibly incorrect T_0 estimates have been considered. An error on the T_0 results in an incorrect evaluation of the time of flight for each photon and causes the $\pi^0\pi^0$ event to be lost. This can occur due to the presence of machine background clusters, which determine the value of T_0 in 1-2% of the events. The uncertainty in R_{acc} (Sec. II) therefore gives rise to a systematic error on the acceptance for $\pi^0\pi^0$ events. However, the acceptance for $\pi^+\pi^-$ events is also affected by an error on R_{acc} , because drift times are wrongly evaluated when T_0 is incorrect. The two effects partially cancel out when evaluating the ratio

of $\pi^+\pi^-$ and $\pi^0\pi^0$ acceptances, leaving a residual systematic error of 0.52×10^{-3} at $E_{\text{cr}} = 300$ MeV (Tab. V).

When the T_0 determination is incorrect because two photons hit the same calorimeter cell, or because one photon cluster overlaps with a noisy EMC channel, a further loss of $\pi^0\pi^0$ events occurs. In such cases, the time of the T_0 cluster is badly reconstructed. The fraction of events lost because of these mechanisms is $\sim 1\%$. The associated correction has been evaluated from data samples of $K_S \rightarrow \pi^0\pi^0$ events tagged by $K_L \rightarrow \pi^+\pi^-\pi^0$ decays in the DC, which can be selected independently of the T_0 determination. The corresponding systematic error is 0.61×10^{-3} (Tab. V).

The $\pi^0\pi^0$ sample is contaminated mainly by K^+K^- events in which one of the two kaons undergoes a decay to $\pi^\pm\pi^0\pi^0$ near the origin, while the other decays to π^0 's within the DC. If the flight path of this second kaon is between ~ 90 and ~ 160 cm, one of the two photons from a π^0 decay can be taken as a K_{cr} . This probability for this to occur strongly decreases with E_{cr} . The purity C is evaluated from MC and depends on E_{cr} as shown in Tab. III. A systematic error on this estimate comes from the uncertainties on the BR's involved in the decay chains and from the acceptance for $K^\pm \rightarrow \pi^\pm\pi^0\pi^0$. The uncertainty is 0.35×10^{-3} at $E_{\text{cr}} = 125$ MeV and negligible at $E_{\text{cr}} = 300$ MeV (Tab. V). A minor source of background, also included in C , is due to events in which multiple clusters from machine background generate both the K_{cr} tag and three prompt clusters. The residual contamination is evaluated using data; it is 0.13×10^{-3} at $E_{\text{cr}} = 125$ MeV and decreases by a factor of two at $E_{\text{cr}} = 300$ MeV. The systematic error due to these events is conservatively estimated to be equal to the contamination itself.

E_{cr} value	125 MeV	200 MeV	300 MeV
N	811,800	587,700	312,900
a_{cr}	0.8905(7)	0.8911(8)	0.8910(9)
C	0.9940(1)	0.99761(8)	0.99938(6)

TABLE III: Values for the observed yield, the acceptance, and the purity of the $\pi^0\pi^0$ selection, for data sample no. 10 and minimum K_{cr} energies of 125, 200, and 300 MeV. Statistical errors on the last digit are shown in parentheses.

E. Trigger, cosmic-ray veto, and offline filter efficiencies

The trigger efficiency for each channel is obtained from data. The trigger requires at least two fired sectors in the EMC and this condition can be satisfied by K_S decay products or by the K_{cr} alone. The idea is therefore to extract the probability $P_{L(S)}^{(i)}$ for the $K_L(K_S)$ to fire i trigger sectors by requiring that the trigger condition be satisfied by the set of $K_S(K_L)$ clusters, which are identified on the basis of the time of flight. The trigger

efficiency is then calculated by combining K_S and K_L trigger sector probabilities. K_L interactions always fire at least one sector, so $P_L^{(2)} = 1 - P_L^{(1)}$. Events are lost when only one sector is fired by the K_{cr} ($P_L^{(1)} \sim 60\%$) and no K_S decay product complements the K_{cr} cluster to satisfy the trigger:

$$\epsilon_{\text{trg}} = 1 - P_S^{(0)} P_L^{(1)} \quad (7)$$

The trigger efficiency ϵ_{trg} is given in Tab. IV for $\pi^+\pi^-$ and $\pi^0\pi^0$ events, and for the three different values of E_{cr} . The maximal variations in ϵ_{trg} during data taking are 0.5% and 0.1%, respectively, and are due to variations in the energy threshold of the calorimeter trigger (related to small changes in the gain of the calorimeter photomultipliers). The systematic error is evaluated using MC events as the difference between the result given by the above method and the MC truth. It is 0.25×10^{-3} for $\pi^+\pi^-$ events with $E_{cr} = 300$ MeV, and negligible for $\pi^0\pi^0$.

The contribution of accidental clusters to the trigger gives an additional systematic error. This is important only for the $\pi^+\pi^-$ channel, for which the trigger inefficiency is $\sim 1.3\%$, as opposed to $\sim 0.1\%$ for $\pi^0\pi^0$. This has been studied using an independent estimate of the trigger efficiency for $\pi^+\pi^-$ events, which is obtained by weighting MC kinematics with data-extracted trigger-sector efficiencies. In contrast to the method for determining the trigger efficiency described above, this method does not include the possible contribution to the trigger from accidental clusters. The difference between the results from the two methods is 0.62×10^{-3} ; this is taken as a further systematic error on the trigger efficiency.

The overall systematic error on the ratio of trigger efficiencies is 0.67×10^{-3} at $E_{cr} = 300$ MeV (Tab. V).

The cosmic-ray veto causes $\sim 3.5\%$ of the events selected with a K_{cr} tag to be lost. The difference between veto efficiencies for $\pi^+\pi^-$ and $\pi^0\pi^0$ events is very small, since in the majority of the rejected events the K_{cr} cluster satisfies the cosmic-ray veto by depositing energy in two adjacent sectors of the outermost EMC layer, and this is independent of the K_S decay channel. Nevertheless, veto efficiencies are evaluated for each channel using a subsample of selected events for which the cosmic-ray veto was present but not enforced at acquisition. The cosmic-ray veto efficiency ϵ_{CV} is given in Tab. IV for $\pi^+\pi^-$ and $\pi^0\pi^0$. The maximal variation in these efficiencies during data taking is $\sim 4 \times 10^{-3}$. The statistical error on the ratio of $\pi^+\pi^-$ and $\pi^0\pi^0$ efficiencies is $\sim 0.2 \times 10^{-3}$ and is included in the statistical error on the efficiency corrections (Tab. V).

The background-rejection filter FILFO makes use of EMC cluster properties and the number of DC hits and is intended to eliminate machine-background or cosmic-ray events before DC reconstruction. The ratio of FILFO efficiencies for $\pi^+\pi^-$ and $\pi^0\pi^0$ events is estimated by MC to be different from unity by $\sim 0.7 \times 10^{-3}$ at $E_{cr} = 300$ MeV. Since FILFO is based on variables with distributions depending on the run conditions, such as the number of DC

hits and the fraction of DC hits in the innermost DC layers, the reliability of this prediction has been checked by studying a data subsample for which the FILFO decision is registered but not enforced during reconstruction. The ratio of FILFO efficiencies for $\pi^+\pi^-$ and $\pi^0\pi^0$ events in data is found to be different from unity by less than 10^{-4} (Tab. IV), and is used to correct the prediction from MC. The systematic error on the ratio of FILFO efficiencies is assumed to be equal to the ratio predicted by MC, which is 0.74×10^{-3} at $E_{cr} = 300$ MeV (Tab. V).

E_{cr} value		125 MeV	200 MeV	300 MeV
$\pi^+\pi^-$	ϵ_{trg}	0.9863(1)	0.9867(1)	0.9879(2)
	ϵ_{CV}	0.9646(3)	0.9626(4)	0.9598(6)
	ϵ_{FILFO}	0.99964(2)	0.99963(3)	0.99944(4)
$\pi^0\pi^0$	ϵ_{trg}	0.99948(3)	0.99948(3)	0.99951(4)
	ϵ_{CV}	0.9625(9)	0.959(1)	0.954(2)
	ϵ_{FILFO}	0.99956(3)	0.99953(3)	0.99937(5)

TABLE IV: Values for the trigger, cosmic-ray veto, and FILFO efficiencies for $\pi^+\pi^-$ and $\pi^0\pi^0$ events, for data sample no. 10 and minimum K_{cr} energies of 125, 200, and 300 MeV. Statistical errors on the last digit are shown in parentheses.

V. RESULTS

The ratio $N(\pi^+\pi^-)/N(\pi^0\pi^0)$ for $E_{cr} = 300$ MeV is shown in the top panel of Fig. 12. The data have been divided into 17 samples of comparable statistical weight; the first six samples correspond to data collected during 2001, samples from 7 to 16 were acquired during 2002, and the last sample refers to data from a dedicated scan performed by varying the center of mass energy by ± 3 MeV around the ϕ peak. The variations observed for $N(\pi^+\pi^-)/N(\pi^0\pi^0)$ are significantly greater than the statistical fluctuations and are due to variations in the overall efficiencies. The most sizable corrections appearing in the ratio of $\pi^0\pi^0$ and $\pi^+\pi^-$ selection efficiencies of Eq. 4 are shown in the first five panels of Fig. 13: these are the acceptances for $\pi^0\pi^0$ and $\pi^+\pi^-$ events, the ratio of trigger and cosmic-ray veto efficiencies, and the tagging-efficiency factor $A(\pi^+\pi^-)$. The variations observed are more pronounced for the samples collected during 2001, for which the rates of machine background were higher and more unstable than for 2002. These have particularly affected the DC efficiency for the innermost layers, and therefore the $\pi^+\pi^-$ acceptance.

Each measurement of R_S^π is obtained by correcting the number of $\pi^+\pi^-$ and $\pi^0\pi^0$ events by the ratio of the selection efficiencies and the background contaminations (Eq. 2) shown in the sixth panel of Fig. 13. In order to avoid statistical correlations between the event counts and the efficiency corrections evaluated from data, each sample has been split into three parts on a random basis. The first of these is used for event counting, the second

for the calculation of the tagging efficiency, and the third for the evaluation of the trigger efficiency. The result for R_S^π is shown in the bottom panel of Fig. 12; the error bars represent the total statistical error, which for most of the samples corresponds to a fractional uncertainty of $\sim 4 \times 10^{-3}$. The χ^2 probability of the fit to a constant is 62%. All quantities entering into the measurement of R_S^π are listed in Tabs. I to IV.

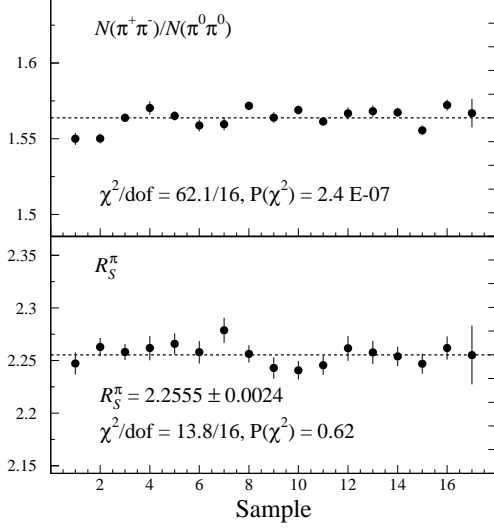


FIG. 12: Ratio $N(\pi^+\pi^-)/N(\pi^0\pi^0)$ (top) and result for R_S^π (bottom) for $E_{\text{cr}} = 300 \text{ MeV}$, for 17 data samples. The fractional vertical range for both plots is 10%, so that each tick on the right vertical axis corresponds to 1%. The error bars represent the total statistical error. The results of fits of $N(\pi^+\pi^-)/N(\pi^0\pi^0)$ and R_S^π to constants and the associated χ^2 values are also shown.

The systematic errors have been evaluated for each sample separately and then averaged by weighting the result from each sample with the corresponding statistical error. The various contributions to the total statistical and systematic errors are shown in Tab. V for K_{cr} minimum energies of 125, 200, and 300 MeV; the “syst-stat” error listed in the second row refers to the statistical uncertainty from all of the corrections; all of the sources of systematic error have been discussed in the previous sections.

The final result is obtained by choosing the value of E_{cr} which minimizes the total error. The best accuracy is obtained for a cut of 300 MeV (see Tab. V). The result is:

$$R_S^\pi = 2.2555 \pm 0.0012_{\text{stat}} \pm 0.0021_{\text{syst-stat}} \pm 0.0050_{\text{syst}}, \quad (8)$$

where the first error is from the statistics of $\pi^+\pi^-$ and $\pi^0\pi^0$ events, the second is due to the statistical error in estimating all of the corrections, and the last is the systematic uncertainty; again it must be emphasized that the error from event counting refers to one third of the total available sample.

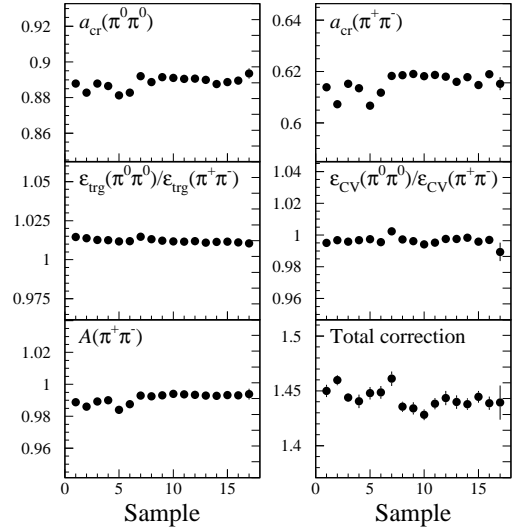


FIG. 13: Most significant efficiency corrections and total correction applied to the ratio $N(\pi^+\pi^-)/N(\pi^0\pi^0)$ for $E_{\text{cr}} = 300 \text{ MeV}$, for 17 data samples. The fractional vertical range for both plots is 10%, so that each tick on the right vertical axis corresponds to 1%. The error bars represent the total statistical error.

Some of the corrections show variations as a function of E_{cr} : the most important of these are the tagging efficiencies [ϵ_{cr} and $A(\pi^+\pi^-)$, Tab. I], and the contamination in the $\pi^0\pi^0$ selection (C , Tab. III). In order to check the reliability of these corrections, the results of the analysis are compared when choosing E_{cr} values of 125, 200, and 300 MeV. Note that the event yield decreases by a factor of three in going from 125 to 300 MeV. In order to avoid correlation effects in the comparison, the data set has been split using a finer granularity, corresponding to 94 samples, each of $\sim 5 \text{ pb}^{-1}$ of integrated luminosity. The analysis is performed using a different energy cut on each successive sample. The χ^2 of the three values obtained has a probability of 21% (see Tab. VI).

The present result (Eq. 8) can be compared with the KLOE result from the analysis of the year 2000 data sample [4],

$$R_S^\pi = 2.236 \pm 0.003_{\text{stat}} \pm 0.015_{\text{syst}}, \quad (9)$$

where in this case the systematic error includes the statistical error from all of the corrections: $0.015 = 0.008_{\text{syst-stat}} \oplus 0.013_{\text{syst}}$. The error on the former result was dominated by the systematic uncertainty on the ratio of tagging efficiencies (0.011). The present analysis makes use of various improvements to the evaluation of the tagging efficiencies with respect to the analysis scheme of Ref. 4: a larger window in β^* is required and a more complete parametrization of the biases induced by errors in the T_0 evaluation has been included. As a result, the absolute systematic error due to the tagging efficiencies has been reduced to 0.0014. The systematic uncertainty due to other sources have been reduced as

E_{cr} value		125 MeV	200 MeV	300 MeV
Source		Fractional statistical error, (10^{-3})		
Event count, “stat”		0.34	0.40	0.54
Efficiencies, “syst-stat”		0.55	0.65	0.93
Total statistical		0.64	0.76	1.1
Source		Fractional systematic error, (10^{-3})		
$\pi^+\pi^-$	K_S - K_L interference	0.80	0.80	0.80
	ϵ_{T0} correction	2.0	1.8	1.4
	Background	0.10	0.10	0.10
$\pi^0\pi^0$	Cluster counting	0.78	0.61	0.66
	Wrong T_0 from K_S	0.60	0.60	0.61
	Physics background	0.35	0.14	0.04
	Machine background	0.13	0.09	0.07
$\pi^+\pi^-/\pi^0\pi^0$	Accidental rate R_{acc}	0.47	0.48	0.52
	$f_n, P_n^{\text{in}}, P_n^{\text{out}}$ evaluation	0.67	0.53	0.45
	ϵ_{cr}	0.39	0.62	0.44
	Trigger	0.91	0.78	0.67
	FILFO	0.45	0.46	0.74
Total systematic		2.8	2.5	2.2
Total		2.8	2.6	2.5

TABLE V: Contributions to the statistical and systematic uncertainties, for minimum K_{cr} energies of 125, 200, and 300 MeV; the “syst-stat” error refers to the statistical uncertainty from all corrections; all sources of systematic error have been discussed in section IV.

K_{cr} energy cut (MeV)	125	200	300
R_S^π	2.2574 ± 0.0025	2.2519 ± 0.0027	2.2590 ± 0.0040
$\chi^2/\text{dof}; \quad P(\chi^2)$	3.12/2; 21%		

TABLE VI: Values of R_S^π for K_{cr} energy cuts of 125, 200, and 300 MeV, obtained from three independent samples, each with 1/3 of the entire statistics. The errors include both the “stat” and “syst-stat” contributions, as defined in the text. The χ^2 value of a fit to a constant and its probability are also shown.

well, from 0.0069 to 0.0048. Nevertheless, the most significant change in the analysis with respect to that described in Ref. 4 is the improved treatment of the tag bias. Therefore, when comparing the two results, the statistical errors and the systematic errors on the tagging efficiencies are treated as independent errors. With this assumption, the two results are compatible, with a probability of 18%. The two measurements can therefore be averaged. Weighting each by its independent errors and calculating the average systematic error with the same weights gives:

$$R_S^\pi = 2.2549 \pm 0.0054. \quad (10)$$

In Ref. 1, this result is combined with the KLOE measurements of $\Gamma(K_S \rightarrow \pi^\mp e^\pm \nu(\bar{\nu}))/\Gamma(K_S \rightarrow \pi^+\pi^-(\gamma))$ to extract the dominant K_S BR’s. To this end, we exploit unitarity: the sum of the BR’s for the $\pi\pi$ and $\pi l\nu$ modes has been assumed to be equal to one, the remaining decays accounting for less than 10^{-4} . The BR of the decay

$K_S \rightarrow \pi\mu\nu$ has been evaluated from the KLOE measurement of $\text{BR}(K_S \rightarrow \pi e\nu)$ and lepton universality. All the results are summarized in the Appendix A. For the $\pi\pi$ modes, we find:

$$\begin{aligned} \text{BR}(K_S \rightarrow \pi^+\pi^-(\gamma)) &= (69.196 \pm 0.051)\% \\ \text{BR}(K_S \rightarrow \pi^0\pi^0) &= (30.687 \pm 0.051)\% \end{aligned} \quad (11)$$

The KTeV collaboration, using their measurement of the ratio of BR’s for the K_L , $R_L^\pi = 2.283 \pm 0.034$, together with the world average for $\Re(\epsilon'/\epsilon)$, $\Re(\epsilon'/\epsilon) = (1.67 \pm 0.26) \times 10^{-3}$, quotes an expected value of R_S^π [18]: $R_S^\pi = 2.261 \pm 0.033$. This is in good agreement with the present result, Eq. 10.

Acknowledgments

We thank the DAΦNE team for their efforts in maintaining low-background running conditions and their col-

laboration during all data taking. We want to thank our technical staff: G. F. Fortugno for his dedicated work to ensure efficient operations of the KLOE Computing Center; M. Anelli for his continuous support to the gas system and the safety of the detector; A. Balla, M. Gatta, G. Corradi, and G. Papalino for the maintenance of the electronics; M. Santoni, G. Paoluzzi, and R. Rosellini for general support to the detector; C. Piscitelli for his help during major maintenance periods. This work was supported in part by DOE grant DE-FG-02-97ER41027; by EURODAPHNE, contract FMRX-CT98-0169; by the German Federal Ministry of Education and Research (BMBF) contract 06-KA-957; by Graduiertenkolleg 'H.E. Phys. and Part. Astrophys.' of Deutsche Forschungsgemeinschaft, Contract No. GK 742; by INTAS, contracts 96-624, 99-37.

APPENDIX A: EVALUATION OF K_S BR'S

The main K_S BR's are evaluated from the measurements of R_S^π and from the ratio of BR's $R_{e\pm} \equiv \text{BR}(K_S \rightarrow \pi^\mp e^\pm \nu(\bar{\nu}))/\text{BR}(K_S \rightarrow \pi^+ \pi^-(\gamma))$. The measured values are [1]:

$$\begin{aligned} R_{e+} &= (5.099 \pm 0.082_{\text{stat}} \pm 0.039_{\text{syst}}) \times 10^{-4} \\ R_{e-} &= (5.083 \pm 0.073_{\text{stat}} \pm 0.042_{\text{syst}}) \times 10^{-4} \end{aligned} \quad (\text{A1})$$

The correlation between results for R_{e+} and R_{e-} is 13%. The only remaining mode with a BR large enough to measurably affect the constraint $\sum_f \text{BR}(K_S \rightarrow f) = 1$ is $K_{\mu 3}$; the BR's for all other channels sum up to $\sim 10^{-5}$.

Assuming lepton universality,

$$r_{\mu e} = \frac{\text{BR}(K_S \rightarrow \pi \mu \nu)}{\text{BR}(K_S \rightarrow \pi e \nu)} = \frac{1 + \delta_K^\mu I_K^\mu}{1 + \delta_K^e I_K^e}, \quad (\text{A2})$$

where $\delta_K^{\mu,e}$ are mode-dependent long-distance radiative corrections and $I_K^{\mu,e}$ are decay phase-space integrals. Using $I_K^\mu/I_K^e = 0.6622(18)$ from KTeV [19] and $(1 + \delta_K^\mu)/(1 + \delta_K^e) = 1.0058(10)$ from Ref. 20, a value for $r_{\mu e}$ is obtained: $r_{\mu e} = 0.6660(19)$. The four main BR's of the K_S are evaluated from

$$\text{BR}(K_S \rightarrow i) = \frac{\Gamma(K_S \rightarrow i)/\Gamma(K_S \rightarrow \pi^+ \pi^-(\gamma))}{1 + 1/R_S^\pi + (R_{e+} + R_{e-})(1 + r_{\mu e})}, \quad (\text{A3})$$

where $i = \pi^+ \pi^-, \pi^0 \pi^0, \pi^- e^+ \nu, \pi^+ e^- \bar{\nu}$. The result is:

$$\begin{aligned} \text{BR}(K_S \rightarrow \pi^+ \pi^-(\gamma)) &= (69.196 \pm 0.051) \times 10^{-2} \\ \text{BR}(K_S \rightarrow \pi^0 \pi^0) &= (30.687 \pm 0.051) \times 10^{-2} \\ \text{BR}(K_S \rightarrow \pi^- e^+ \nu) &= (3.528 \pm 0.062) \times 10^{-4} \end{aligned} \quad (\text{A4})$$

$$\begin{aligned} \text{BR}(K_S \rightarrow \pi^+ e^- \bar{\nu}) &= (3.517 \pm 0.058) \times 10^{-4} \\ \text{The correlation matrix } \langle \delta_i \delta_j \rangle / \sqrt{\langle \delta_i^2 \rangle \langle \delta_j^2 \rangle} &\text{ is} \end{aligned}$$

$$\begin{array}{c} \pi^+ \pi^- \\ \pi^0 \pi^0 \\ \pi^- e^+ \nu \\ \pi^+ e^- \bar{\nu} \end{array} \begin{pmatrix} \pi^+ \pi^- & \pi^0 \pi^0 & \pi^- e^+ \nu & \pi^+ e^- \bar{\nu} \\ 1 & -0.9996 & 0.0254 & 0.0294 \\ -0.9996 & 1 & -0.0484 & -0.0511 \\ 0.0254 & -0.0484 & 1 & 0.1320 \\ 0.0294 & -0.0511 & 0.1320 & 1 \end{pmatrix} \quad (\text{A5})$$

-
- [1] KLOE Collaboration, F. Ambrosino, *et al.*, **hep-ex/0601026**, accepted for publication by Phys. Lett. B.
 - [2] V. Cirigliano, J. F. Donoghue, and E. Golowich, Eur. Phys. J. **C18**, 83 (2000).
 - [3] V. Cirigliano, G. Ecker, H. Neufeld, and A. Pich, Eur. Phys. J. **C33**, 369 (2004).
 - [4] KLOE Collaboration, A. Aloisio *et al.*, Phys. Lett. **B538**, 21 (2002).
 - [5] D. E. Groom *et al.* (Particle Data Group), Eur. Phys. J. **C15**, 1 (2000).
 - [6] S. Eidelman, *et al.*, Particle Data Group, Phys. Lett. **B592** (2004), and 2005 partial update for edition 2006, URL <http://pdg.lbl.gov>.
 - [7] I. Dunietz, J. Hauser, and J. Rosner, Phys. Rev. **D35**, 2166 (1987).
 - [8] N. Paver and Riazuddin, Phys. Lett. **B246**, 240 (1990).
 - [9] F. E. Close, N. Isgur, and S. Kumano, Nucl. Phys. **B389**, 513 (1993).
 - [10] KLOE Collaboration, M. Adinolfi, *et al.*, Nucl. Instr. and Meth. **A488**, 51 (2002).
 - [11] I. Navon *et al.*, Phys. Rev. **C22**, 717 (1980).
 - [12] KLOE Collaboration, M. Adinolfi, *et al.*, Nucl. Instr. and Meth. **A482**, 363 (2002).
 - [13] KLOE Collaboration, M. Adinolfi, *et al.*, Nucl. Instr. and Meth. **A492**, 134 (2002).
 - [14] KLOE Collaboration, F. Ambrosino *et al.*, Nucl. Instr. and Meth. **A534**, 403 (2004).
 - [15] C. Gatti, M. Palutan, and T. Spadaro, KLOE Note 209 (2006), unpublished, URL <http://www.lnf.infn.it/kloe/pub/knote/kn209.ps>.
 - [16] C. Gatti, Eur. Phys. J. **C45**, 417 (2005), and references therein.
 - [17] E. Ramberg *et al.*, Phys. Rev. Lett. **70**, 2525 (1993).
 - [18] KTeV Collaboration, T. Alexopoulos, *et al.*, Phys. Rev. **D70**, 092006 (2004).
 - [19] KTeV Collaboration, T. Alexopoulos, *et al.*, Phys. Rev. **D70**, 092007 (2004).
 - [20] T. C. Andre (2004), **hep-ph/0406006**.